

Fast high-resolution metabolite mapping in the rat brain using ^1H -FID-MRSI at 14.1 T

Dunja Simicic^{1,2*}, Brayan Alves^{1,2*}, Jessie Mosso^{1,2,3}, Guillaume Briand^{1,2}, Thanh Phong Lê³, Ruud B. van Heeswijk⁴, Jana Starčuková⁵, Bernard Lanz^{1,2}, Antoine Klauser⁶, Bernhard Strasser⁷, Wolfgang Bogner⁷, Cristina Cudalbu^{1,2}

¹ CIBM Center for Biomedical Imaging, Switzerland

² Animal Imaging and Technology, École polytechnique fédérale de Lausanne (EPFL), Lausanne, Switzerland

³ Laboratory of Functional and Metabolic Imaging, École polytechnique fédérale de Lausanne (EPFL), Lausanne, Switzerland

⁴ Department of Diagnostic and Interventional Radiology, Lausanne University Hospital (CHUV) and University of Lausanne (UNIL), Lausanne, Switzerland

⁵ Institute of Scientific Instruments of the CAS, Brno, Czech Republic

⁶ Advanced Clinical Imaging Technology, Siemens Healthcare AG, Lausanne, Switzerland

⁷ High-field MR Center, Department of Biomedical Imaging and Image-guided Therapy, Medical University Vienna, Vienna, Austria

*Joint first authors

Word count: 5833

Corresponding author: Dunja Simicic (dunja.simicic@epfl.ch), Cristina Cudalbu (cristina.cudalbu@epfl.ch)

Keywords: magnetic resonance spectroscopic imaging, ^1H -FID-MRSI, rat brain, ultra-high field, metabolite mapping, brain metabolites

Abbreviations:

MRSI - Magnetic Resonance Spectroscopic Imaging, FID - Free Induction Decay, AD - Acquisition Delay, TR - Repetition Time, SVD - Singular Value Decomposition, SNR - Signal to Noise Ratio, SD - Standard Deviation, FWHM - Full Width at Half Maximum, FT - Fourier Transform, NAA - N-Acetyl Aspartate, NAAG - N-acetylaspartyglutamate, Ins - myo-Inositol, Gln - Glutamine, Glu - Glutamate, GABA - Gamma-Aminobutyric Acid, Asp - Aspartic Acid, Ala - Alanine, Asc - Ascorbic Acid, Cr - Creatine, PCr - Phosphocreatine, tCr - total Creatine, Tau - Taurine, PCho - Phosphocholine, GPC - Glycerophosphocholine, PE - Phosphoethanolamine, Lac - Lactate, Glc - Glucose, GSH - Glutathione

Abstract:

Magnetic resonance spectroscopic imaging (MRSI) enables the simultaneous non-invasive acquisition of MR spectra from multiple spatial locations inside the brain. While ^1H -MRSI is increasingly used in the human brain, it is not yet widely applied in the preclinical setting, mostly because of difficulties specifically related to very small nominal voxel size in the rodent brain and low concentration of brain metabolites, resulting in low signal-to-noise ratio SNR.

In this context, we implemented a free induction decay ^1H -MRSI sequence (^1H -FID-MRSI) in the rat brain at 14.1T. We combined the advantages of ^1H -FID-MRSI with the ultra-high magnetic field to achieve higher SNR, coverage and spatial resolution in the rodent brain, and developed a custom dedicated processing pipeline with a graphical user interface for Bruker ^1H -FID-MRSI: *MRS4Brain toolbox*.

LCModel fit, using the simulated metabolite basis-set and in-vivo measured MM, provided reliable fits for the data at acquisition delays of 1.3 and 0.94 ms. The resulting Cramér-Rao lower bounds were sufficiently low (<40%) for eight metabolites of interest, leading to highly reproducible metabolic maps. Similar spectral quality and metabolic maps were obtained between 1 and 2 averages, with slightly better contrast and brain coverage due to increased SNR in the latter case. Furthermore, the obtained metabolic maps were accurate enough to confirm the previously known brain regional distribution of some metabolites. The acquisitions proved high repeatability over time.

We demonstrated that the increased SNR and spectral resolution at 14.1T can be translated into high spatial resolution in ^1H -FID-MRSI of the rat brain in 13 minutes, using the sequence and processing pipeline described herein. High-resolution ^1H -FID-MRSI at 14.1T provided robust, reproducible and high-quality metabolic mapping of brain metabolites with significantly reduced technical limitations.

1. Introduction

Magnetic resonance spectroscopic imaging (MRSI) enables the simultaneous non-invasive acquisition of MR spectra from multiple spatial locations inside the brain. Even though such mapping of the metabolic regional differences in-vivo is very valuable for both clinical and preclinical research, the routine application of MRSI remains challenging due to several issues. These include long acquisition times, low signal-to-noise ratio (SNR), the need to develop in-house acquisition sequences and processing pipelines, the huge amount of data that needs to be handled, etc.¹ The availability of ultra-high magnetic fields (UHF) and the corresponding increase in SNR and spectral dispersion, combined with advanced pulse sequences and new encoding methods, improved the quality and speed of MRSI^{2,3} specifically for human studies. At UHF, in the clinical settings, free induction decay (¹H-FID-MRSI) acquisitions are increasingly used². FID-MRSI acquisition minimizes the T₂ relaxation and eliminates J-evolution. This in turn increases the SNR and potentially the number of detected metabolites. It also reduces chemical shift displacement errors and sensitivity to B₀ inhomogeneity³⁻⁶. Moreover, this simple sequence design permits a considerable acquisition time reduction by decreasing the repetition time (TR) while using an optimal Ernst's flip angle.

While ¹H-MRSI is increasingly used in the human brain, it is not yet widely applied in the preclinical settings, mostly because of difficulties specifically related to the small rodent brain⁷. The resulting low SNR arises from the low concentration of brain metabolites combined with a very small nominal voxel size in rodents (e.g. 0.75 × 0.75 × 2 mm³ in a 32 × 32 matrix)⁸, while in the human brain the nominal voxel size remains fairly large even at high spatial resolution (e.g. 1.7 × 1.7 × 10 mm³, for a 128 × 128 matrix)⁹. Furthermore, there are additional challenges in terms of shimming of large volumes with many tissue interfaces, long measurement times with traditional MRSI sequences (e.g 120 minutes)^{8,10,11}, water suppression artifacts and lipid contamination.⁷ These are combined with the need to develop automatic and standardized processing pipelines, to perform quality assessment of a very large number of spectra and to estimate the precision and reliability of derived metabolite maps. To the best of our knowledge, at the present time traditional phase encoded MRSI using STEAM, PRESS or SPECIAL excitation schemes (at TEs between 2-10 ms), is still used for quantitative mapping of an extended number of metabolites^{8,12,13}, while no advanced processing and quality control pipelines are available for FID-MRSI Bruker data. Fast MRSI has been implemented for hyperpolarized molecular imaging, however under very different conditions and constraints (intense but quickly decaying signal, typically lower spatial resolution, very few metabolites with almost no overlap¹⁴).

In this context, we propose the implementation of ¹H-FID-MRSI in the rat brain at 14.1T, something novel in the preclinical setting. We combined the advantages of ¹H-FID-MRSI acquisitions with the UHF of 14.1T to achieve higher SNR and spatial resolution in the rodent brain. Furthermore, as MRSI acquisitions are characterized by a very large amount of data that needs to be

processed and subjected to quality control to reliably estimate and derive metabolite maps, we implemented a custom dedicated processing pipeline for Bruker ^1H -FID-MRSI able to perform water and lipid suppression, fitting, semi-automatic quality assessment, atlas-based segmentation, and an overlay of metabolic maps on the corresponding anatomical MRI image; all these are incorporated in a user-friendly toolbox with a graphical user interface (GUI).

2. Methods

All experiments were approved by The Committee on Animal Experimentation for the Canton de Vaud, Switzerland (VD 3022.1). Wistar male adult rats ($n = 10$ rats, 240 ± 50 g, Charles River Laboratories, L'Arbresle, France) under 1.5-2.5% isoflurane anesthesia were used. The body temperature of the animals was kept at 37.5 ± 1.0 °C by circulating warm water and measured with a rectal thermosensor. The respiration rate and body temperature were monitored using a small-animal monitor system (SA Instruments, New York, NY, USA). During the MRI scans all animals were placed in an in-house-built holder, with their head fixed in a stereotaxic system using a bite bar and a pair of ear bars.

2.1 Two-compartment phantom and in-vivo ^1H -MRSI acquisitions

Fast ^1H -FID-MRSI measurements were performed in the rat brain on a 14.1T horizontal magnet (Magnex Scientific, Yarnton, UK), a 1 T/m peak strength and 5500 T/m/s slew rate shielded gradient set (Resonance Research, Billerica, USA) interfaced to a Bruker console (BioSpec Avance NEO, ParaVision 360 v1.1 and v3.3), and using a home-made transmit/receive quadrature surface coil (20 mm inner diameter).

T_2 -weighted Turbo-RARE images were acquired in coronal and axial direction to position the MRSI slice for shimming, acquisition and for metabolic maps overlays (20 slices, TR = 3000 ms, $TE_{eff} = 27$ ms, NA = 2, RARE_{factor} = 6, 256×256 matrix, 0.8 mm slice thickness, FOV = 24×24 mm 2). A second T_2 -weighted Turbo-RARE image was acquired in each rat for brain segmentation (60 slices, TR = 4100 ms, $TE_{eff} = 27$ ms, NA = 10, RARE_{factor} = 6, 128×128 matrix, 0.2 mm slice thickness, FOV = 24×24 mm 2).

For the high-resolution two-dimensional fast ^1H -FID-MRSI acquisitions, a slice-selective pulse-acquire sequence was used in combination with VAPOR¹⁵ water suppression and 6 saturation slabs to minimize lipid contamination (Figure 1A). The MRSI slice was centered on the hippocampus, with 2 mm slice thickness and an FOV of 24×24 mm 2 (same FOV as for imaging, Figure 2). The matrix size was 31×31 leading to a nominal voxel size of $0.77 \times 0.77 \times 2$ mm 3 . The following acquisition parameters were used: spectral bandwidth of 7 kHz, 1024 FID data points, Cartesian k -space sampling, 8 dummy scans, acquisition delay (AD) 1.3 ms, TR=813 ms leading to a total measurement time of 13 minutes. The excitation pulse was adjusted to the Ernst angle of 52° (0.5 ms calculated RF pulse with the Shinnar-Le

Roux algorithm). First and second order shims were adjusted using Bruker MAPSHIM, first in an ellipsoid covering the full brain and further in a volume of interest (VOI) of $10 \times 10 \times 2$ mm³ centered on the MRSI slice.

The following acquisitions were performed to validate the implementation of the fast ¹H-FID-MRSI sequence and test the reproducibility of the acquired data:

- To test the precision of the ¹H-FID-MRSI sequence and its ability to separate metabolic profiles from different brain regions a two-compartment phantom was measured using ¹H-FID-MRSI and PRESS-MRSI sequences (for details see Supplementary Material).
- Seven in-vivo datasets with one and two averages, respectively, were acquired on n=6 rats.
- To test the reproducibility and stability of the acquired data, two additional in-vivo measurements were performed:
 - 3 acquisitions with 1 average and 2 acquisitions with 2 averages were performed in an interleaved mode in one rat. Before each scan, the water linewidth was measured and if needed a MAPSHIM was performed in the $10 \times 10 \times 2$ mm³ VOI. The achieved water linewidth was in the range of 24-30 Hz.
 - One rat was scanned twice at 2 weeks interval using 1 and 2 averages.
- The ¹H-FID-MRSI sequence was further improved by reducing the RF pulse and phase encoding durations to 0.2 and 0.3 ms, respectively, which led to an AD of 0.94 ms. Additional in-vivo acquisitions were performed with these new parameters using n = 4 additional rats.

2.2 Processing pipeline, semi-automatic quality control and automatic brain segmentation

A homemade processing pipeline was developed in MATLAB specifically for ¹H-FID-MRSI datasets (Bruker, ParaVision 360 v1.X and v3.X formats). The pipeline was partially inspired by previous human brain ¹H-FID-MRSI processing pipelines¹⁶ and contains the following steps:

1. Data formats: Bruker MRSI datasets already FT in the image space (*fid* for ParaVision 360v1.X and *fid_proc.64* for ParaVision 360v3.X) and further stored in 2D matrices, where each voxel contains one FID.
2. The water power mask was used to filter out the voxels located outside the brain and later for the lipid suppression (step 4 below). The power of the separately acquired water signal was computed by summing the squared magnitude of the frequency-domain signal. The segmentation condition for the water power mask was given by half the mean power over the full slice; a voxel was considered in the brain region if its power was higher than this threshold (Figure 1B). Voxels located inside the brain are further kept for LCModel quantification and quality control.

3. Residual water signal removal from the metabolite signal using a Hankel-Singular Value Decomposition (HSVD) water suppression^{16,17}.
4. SVD-based lipid suppression¹⁶ based on the assumption that lipids and metabolites are orthogonal in the time or frequency and the spatial domain. A brain/scalp segmentation was performed using the water power mask from step 2. The scalp voxels were subsequently used to generate an orthogonal basis for the lipid components by performing an SVD on the lipid voxel data. The rank of the basis was determined by the energy ratio between the brain and the scalp region after application of the projector: $E_{\text{Brain}}/E_{\text{Skull}} \geq \alpha$ (more information in¹⁶), with α being manually set by the user in the pipeline (α was set to 0.5 in the present study).
5. For an overall quality control of the acquired data the following maps were computed: a linewidth and ΔB_0 map (i.e. frequency shifts) using the water signal and an SNR map using the metabolite signal. The SNR was calculated from the NAA (2.01 ppm), defined as the NAA peak height in the magnitude spectrum divided by one standard deviation (SD) of the noise measured in a noise-only region of the real part of the spectrum (from (-0.9) to (-1.25) ppm)¹⁸ (Supplementary Figure 1).
6. LCmodel (Version 6.3-1N) fitting with details provided below.
7. Semi-automatic quality control after fitting: the pipeline uses the values of SNR and FWHM from LCModel and averages both over the number of voxels: *SNR* and *FWHM*. Fixed thresholds for quality filtering were chosen to be set above 75% of *SNR* and below 125% of *FWHM*. An additional acceptance criterion with respect to the Cramer-Rao lower bound of the metabolites located in the voxel was added for the *in-vivo* datasets: for each metabolite, the CRLB was defined to be lower or equal than 40% (Supplementary Figure 1).
8. Creation of metabolite maps overlaid to the corresponding MRI image based on the semi-automatic quality control performed after fitting. For visualization purposes, a bicubic convolution interpolation was used on the metabolic maps.
9. An atlas based automatic segmentation tool was also implemented (Supplementary Figure 2): a multi-steps registration was computed with an anatomical template, created for this purpose and based on the SIGMA atlas¹⁹. The transformation found with registration was applied to the labeled template and the regions can be reshaped to correspond to the MRSI spatial resolution.

Recently, the processing pipeline was incorporated in a MATLAB toolbox with a user-friendly GUI: *MRS4Brain toolbox* (Supplementary Figure 2) with the objective to provide a standardized processing tool for Bruker preclinical MRSI data.

2.3 Fitting and quantification

The spectra contained in the brain region (obtained by brain/scalp segmentation) were quantified using LCModel. The basis-set of metabolites was simulated using NMR Scope-B (18 metabolites) from jMRUI²⁰, using published values of J-coupling constants and chemical shifts^{21,22} and the pulse-acquire

sequence with the same parameters as for the in-vivo ^1H -FID-MRSI metabolite acquisitions (Figure 1C). Two basis-sets were created: one for AD=1.3 ms and the second for AD=0.94 ms. In each basis-set the following metabolites were included: alanine (Ala), aspartate (Asp), ascorbate (Asc), creatine (Cr), phosphocreatine (PCr), γ -aminobutyrate (GABA), glutamine (Gln), glutamate (Glu), glycerophosphocholine (GPC), glutathione (GSH), glucose (Glc), inositol (Ins), N-acetylaspartate (NAA), N-acetylaspartyglutamate (NAAG), phosphocholine (PCho), phosphoethanolamine (PE), lactate (Lac), taurine (Tau). PCho and GPC, and Cr and PCr were expressed only as tCho (PCho + GPC) and tCr (Cr+PCr) due to better accuracy in the estimation of their concentration as a sum.

For the AD = 1.3 ms, the macromolecule (MM) spectrum was first acquired using a single inversion recovery module implemented in the ^1H -FID-MRSI sequence (TI=775 ms, hyperbolic secant *HSI_R20.inv* RF pulse of 2 ms duration, 10×10 matrix size, 10 averages, TR=1500 ms, 2048 FID data points, 7 kHz acquisition bandwidth), but the acquired MM showed an important contamination with residual metabolites which were difficult to reliably identify and fully remove (data not shown). Therefore, the final MM spectrum was acquired using a single inversion recovery STEAM sequence (TI=750 ms, 64 averages, TE=3 ms, TR=1344 ms, *HSI_R20.inv* RF pulse of 2 ms duration, 2048 FID data points, 7 kHz acquisition bandwidth) in the voxel of $10 \times 10 \times 2$ mm 3 centered on the MRSI slice. The metabolite residuals were removed with AMARES from jMRUI as previously described¹⁸. To match the acquisition delay (1st order phase evolution due to the acquisition delay of 1.3 ms) to the one of the metabolites in the basis-set the first points of the FID were removed, and this final MM signal was added to the basis-set (Figure 1C). In order to acquire the MM with the same sequence as for the metabolites, for the AD = 0.94 ms a double inversion recovery module was implemented into the ^1H -FID-MRSI sequence (TI = 2200/850 ms, 15×15 matrix size, 6 averages, TR = 3400 ms, *HSI_R20.inv* RF pulse of 2 ms duration, 2048 FID data points, 7 kHz acquisition bandwidth). Due to low SNR of the acquired MM, six voxels were summed to obtain the final MM signal and the residual water was removed using AMARES²³.

tCr was used as a reference for our model due to the short TR used in the sequence and the T₁relaxation of the metabolites.

2.4 Data display and statistics

All data are presented as mean \pm SD. To evaluate the feasibility of the described ^1H -FID-MRSI sequence to quantify previously known brain regional changes¹⁹, an automatic segmentation of two different brain regions was performed ($n = 4$ rats, AD = 1.3 ms, 2 averages): a region with a mix of striatum and cortex and a region composed of hippocampus, as shown in Supplementary Figure 2. The average concentration in these brain regions was computed by averaging the concentration values over the number of voxels contained in the specific region after performing the semi-automatic quality

control. Ins and Gln were chosen to be presented due to their known regional distribution in the rodent brain²⁴.

Two-way analysis of variance (ANOVA) (Prism 5.04, GraphPad Software, San Diego, CA, USA) with respect to each metabolite in the neurochemical profile followed by Bonferroni's multi-comparisons post-test were performed. Two categorical factors were defined: the brain regions (hippocampus and cortex+striatum) and the number of averages (1 average and 2 averages). For the statistical tests with different AD, the analysis was conducted with the brain regions factor and the different AD (AD=1.3 ms and AD=0.94 ms). The significance level in two-way ANOVA was attributed as follows: *p < .05, **p < .01, ***p < .001, and ****p < .0001. All tests were two-tailed.

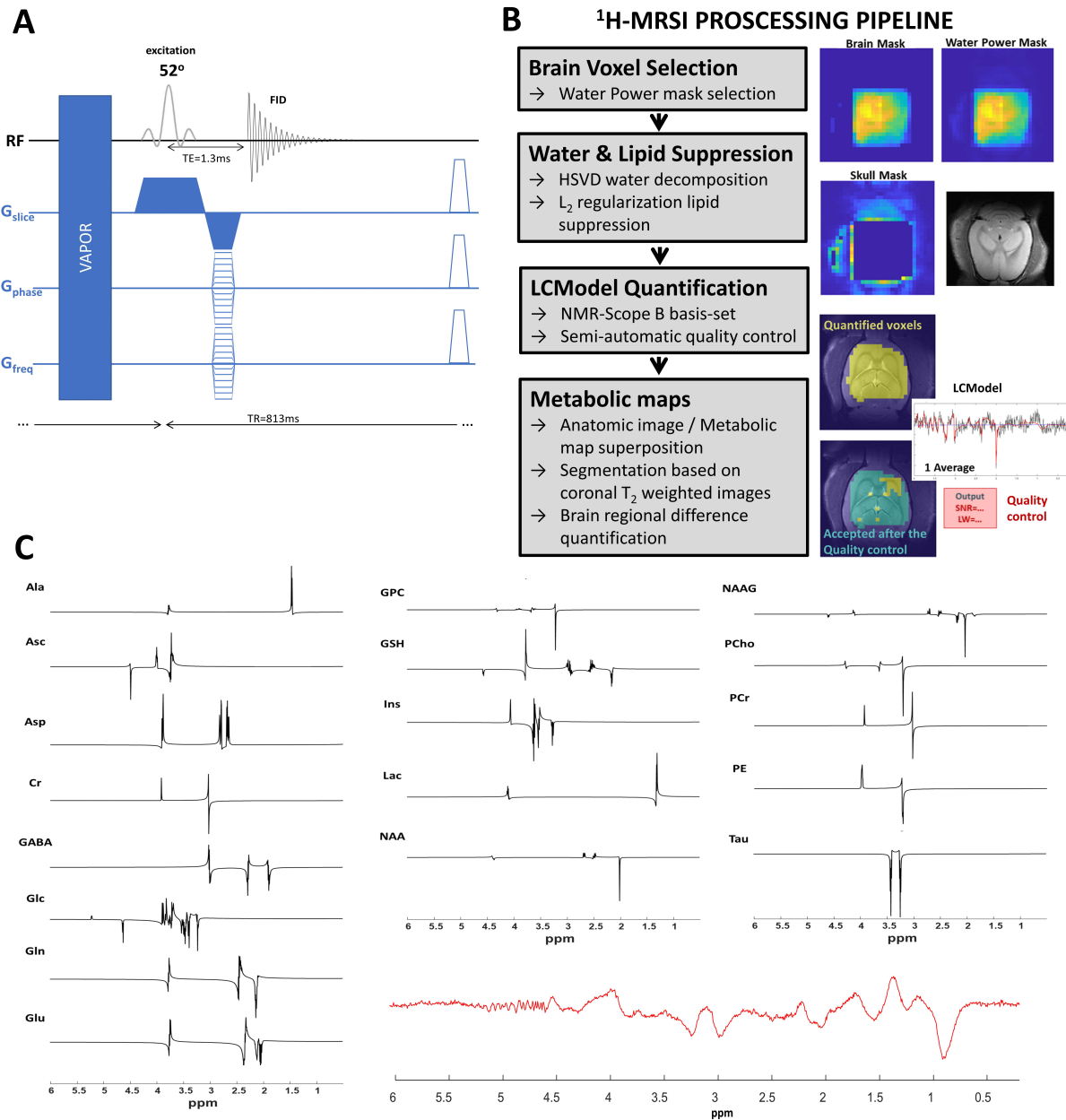


Figure 1 (A) A schematic drawing of the ¹H-FID-MRSI sequence used for data acquisition. (B) Sketch of the processing pipeline used for ¹H-MRSI datasets (C) The metabolites simulated using NMR Scope-B (18 metabolites) from jMRUI and the in-vivo MM included in the basis-set.

3. Results

The performance of the ¹H-FID-MRSI sequence was tested on a two-compartment phantom, in-vivo in the rat brain (n=10) using two different ADs with 1 and 2 averages. In addition, some reproducibility tests were also performed in two rats with a total of 9 measurements with 1 and 2 averages.

3.1 Data quality

The shim adjustments using MAPSHIM, first in an ellipsoid covering the full brain then in a voxel of $10 \times 10 \times 2 \text{ mm}^3$ centered on the MRSI slice, proved to be efficient when shimming in large areas. The average water linewidth over the 10 rats was $28.5 \pm 2.5 \text{ Hz}$, measured in the $10 \times 10 \times 2 \text{ mm}^3$ VOI centered on the MRSI slice. This translated into good quality spectra in a large number of nominal voxels in the MRSI matrix after the application of the water power mask (step 2 in the MRSI processing pipeline), ~230 voxels selected by the water power mask (~25% of the whole slice). Therefore, a large in-plane coverage was achieved extending also towards the edges of the brain and was not limited to a rectangular volume like for PRESS-MRSI. The computed water maps from the two-compartment phantom confirmed the increased in-plane coverage when using the ^1H -FID-MRSI sequence (Supplementary Figure 3). Moreover, the water maps showed that the acquired signal comes from two clearly separated compartments, while the visual comparison of metabolite spectra from different positions in the MRSI matrix highlighted the ability of the ^1H -FID-MRSI sequence to separate metabolic profiles from two closely positioned compartments with different metabolites.

The overall quality assessment computed by step 5 in the MRSI processing pipeline is shown in Supplementary Figure 1, highlighting the quality of the acquired data after automatically filtering out the spectra located outside the brain based on the water power mask (step 2 in the MRSI processing pipeline). As can be seen, the frequency shifts over the investigated MRSI slice (i.e. ΔB_0) were overall below 20 Hz, while they were increased in some parts towards the edges of the MRSI slice. These small water frequency shifts highlighted a good quality shimming as shown in the same figure by the water linewidth map (around 20-30 Hz with broader linewidths in regions with higher ΔB_0). Furthermore, small water frequency shifts are also mandatory for good water suppression during the acquisition of the MRSI datasets. The region containing broader linewidths was further removed by the semi-automatic quality control (step 7 in the MRSI processing pipeline) as shown by the smaller voxel selection afterwards. Despite the small nominal voxel size ($0.77 \times 0.77 \times 2 \text{ mm}^3$) we reproducibly obtained good SNR data. The computed NAA SNR map after step 5 in the processing pipeline resulted in averaged SNR values, over the entire datasets contained in the power mask, ranging from 6.6 ± 2.4 to 8.6 ± 3.5 for the measurements performed with 1 average.

Figure 2 shows an example of spectra acquired with 1 and 2 averages from two distinct locations in the rat brain (left and right hippocampus) and the corresponding LCModel fits. High-quality spectra were acquired with similar spectral quality between 1 and 2 averages and between right and left hippocampus, without baseline distortions due to water residuals or lipid contamination. The averaged metabolite SNR values computed over the entire datasets contained in the power mask increased by 30% for the measurements performed with 2 averages. This SNR increase is an estimate as the data after the power mask selection still need to pass the quality

control (step 7 in the MRSI processing pipeline). Thus, low quality spectra can still be present as highlighted in Supplementary Figure 1B.

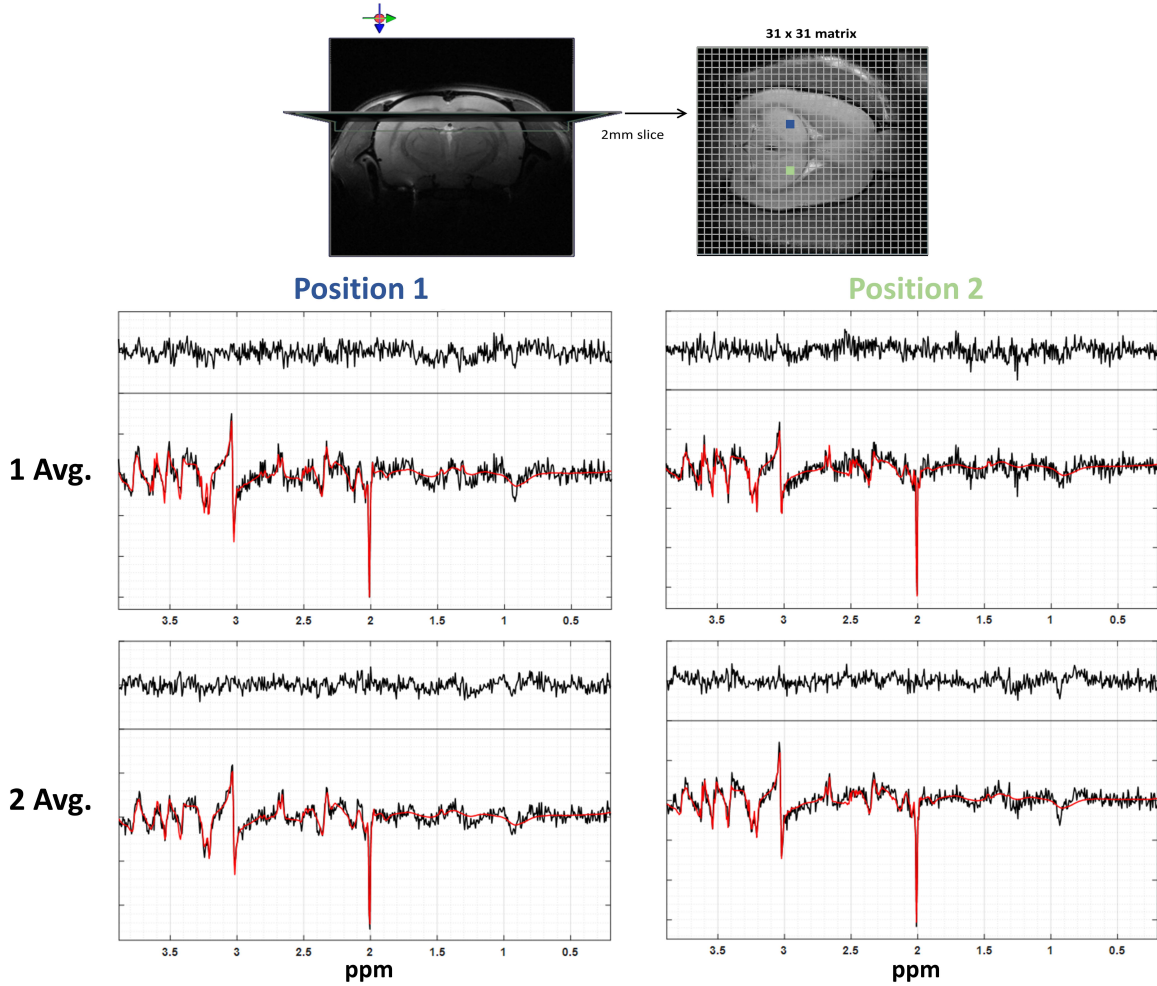


Figure 2 Examples of the MRSI slice position in both axial and coronal views, and the spatial resolution are shown on the upper part of the figure. The high-quality of spectra and of the LCModel fits are shown for spectra from two different positions in the MRSI matrix with one and two averages.

3.2 In-vivo metabolic maps

The LCModel fit, using the simulated metabolite basis-set and in-vivo measured MM, provided reliable fits for the data obtained with both one and two averages at AD=1.3 ms (Figure 2, Supplementary Figure 4). The resulting Cramér-Rao lower bounds (CRLB's) were sufficiently low (<40%) for eight metabolites of interest (tCr, NAA, tNAA, tCho, Gln, Glu, Ins, Tau) leading to reproducible metabolic maps. The metabolic maps overlaid on the corresponding anatomical image for NAA, Glu and tCho are shown in Figure 3 for 1 and 2 averages after the application of the semi-automatic quality control described in the MRSI processing pipeline (step 7). Although the metabolic maps obtained from the acquisition with two averages provided a better contrast and brain coverage

due to increased SNR, the maps kept the same pattern when using one average proving that this very fast acquisition leads to a satisfactory output. As can be seen in Supplementary Figure 1B, the semi-automatic quality control led to the removal of some voxels in some areas where the quality of the spectra did not pass the selection criteria, leading to a slightly different coverage than the one first predicted by the water power mask (51% and 64% of the voxels in the water power mask were accepted for 1 and 2 averages, respectively). Table 1 illustrates the mean concentration estimates on 6 rats (7 measurements) in two different brain regions. The results obtained with 1 and 2 averages are highly reproducible in the investigated brain regions with 2-10% statistically non-significant differences between 1 and 2 averages for the reported metabolites. tCr was used as internal reference due to the T₁ weighting induced by the short repetition time used in the current manuscript.

To illustrate the ability of the described ¹H-FID-MRSI sequence and processing pipeline to quantify previously known brain regional changes, Figure 4 depicts the obtained metabolic maps of Ins and Gln which were accurate enough to confirm the previously known²⁴ brain regional distribution of these metabolites. We quantified up to 34 region specific nominal voxels in the hippocampus and 30 for cortex+striatum. Furthermore, Figure 4C confirms the reproducibility of our MRSI acquisition displaying the Ins and Gln concentration ratios obtained from four different rats, proving the reproducible estimation of these metabolites even with one average (13 minutes).

To further minimize first-order phase problems and signal loss due to AD, we have implemented a new protocol where the AD was reduced at 0.94 ms by decreasing the duration of the excitation RF pulse and phase encoding. An example of data acquired with this shorter AD is shown in Figure 5. Qualitatively, high reproducibility of metabolic mapping was obtained between AD = 1.3 ms and 0.94 ms, as can be seen when comparing the metabolic maps of NAA, tCho and Glu. An approximate 9% increase in SNR was observed when comparing the averaged metabolite SNR maps between the two ADs ($n = 4$ rats for each AD). The estimated concentrations for 7 metabolites are displayed in Table 2 for the two ADs and two brain regions. On average 5-20 % statistically non-significant difference was measured between the two ADs, which was similar for the two brain regions.

The *MRS4Brain toolbox* with a user-friendly MATLAB-based interface combining all processing steps was developed and used in the current study (Supplementary Figure 2), taking into account the huge amount of data acquired during each scan and the specific needs regarding the processing, artifacts removal when possible, fitting, quality control and display of reliably segmented metabolic maps. Each step of this processing pipeline was described and the results presented herein. The duration of the processing and quantification was estimated to be 10 minutes per dataset.

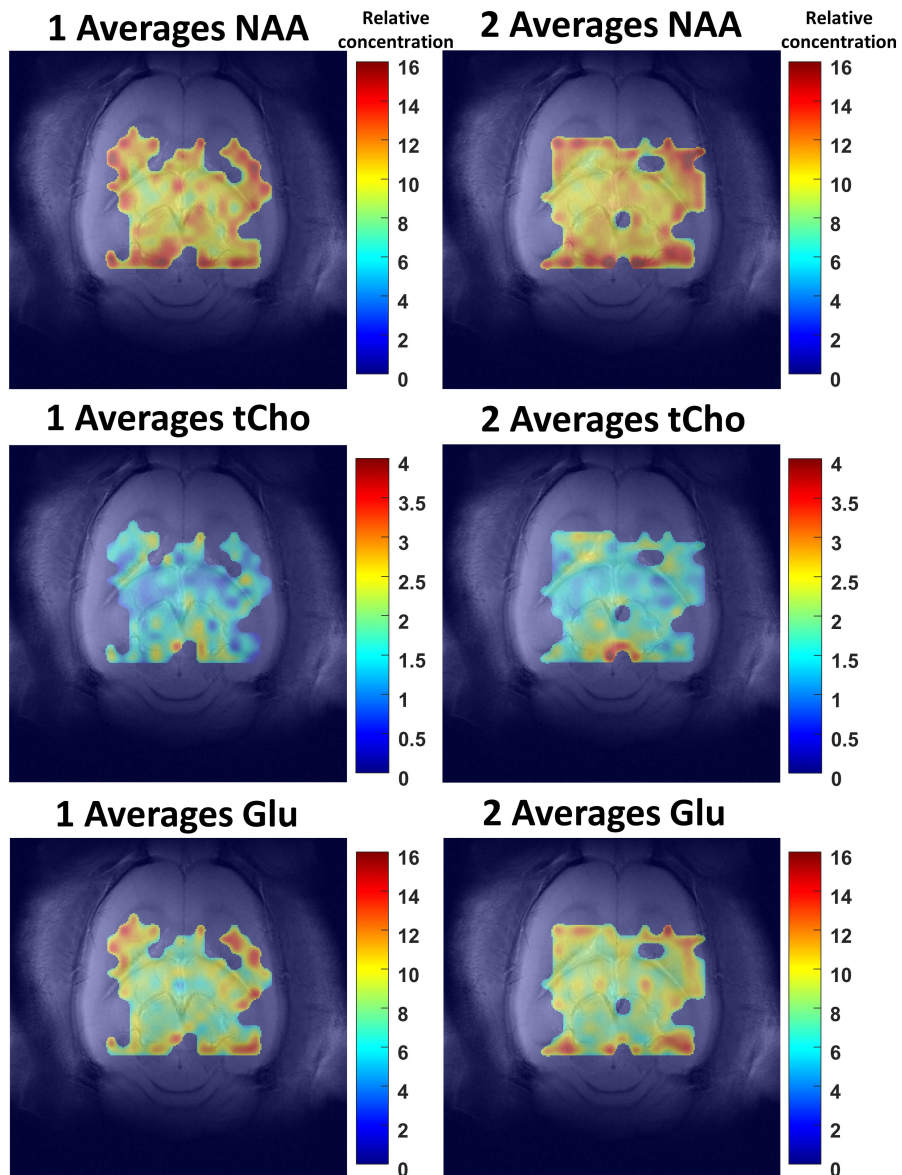


Figure 3. Representative metabolic maps obtained from the LCModel quantification results of the data acquired in one rat with one average (on the left) and two averages (on the right). As can be seen the obtained metabolic maps are similar between 1 and 2 averages, with a better contrast for 2 averages due to an increased SNR. The metabolic maps were superimposed to the corresponding anatomical image using the MRS4Brain toolbox. The scales correspond to LCModel outputs when referenced to tCr by setting its concentration to 8 mmol/kg_{ww}. A bicubic convolution interpolation was used on the metabolic maps.

1 Averages			2 Averages		
*/tCr [mmol/kg _{ww}]	Hippocampus	Striatum + Cortex	*/tCr [mmol/kg _{ww}]	Hippocampus	Striatum + Cortex
NAA	10.94 ± 0.69	11.58 ± 0.84	NAA	10.56 ± 0.55	11.05 ± 0.71
Gln	3.08 ± 0.53	3.54 ± 0.42	Gln	2.99 ± 0.42	3.39 ± 0.37
Glu	9.32 ± 0.73	10.08 ± 0.73	Glu	9.16 ± 0.70	9.62 ± 0.63
Ins	10.43 ± 0.72	8.79 ± 0.74	Ins	9.83 ± 0.86	7.93 ± 0.63
Tau	8.49 ± 0.58	8.79 ± 0.63	Tau	8.69 ± 1.30	8.51 ± 0.56
GPC+PCho	2.17 ± 0.16	2.29 ± 0.21	GPC+PCho	2.11 ± 0.18	2.16 ± 0.20
NAA+NAAG	11.41 ± 0.77	11.91 ± 0.86	NAA+NAAG	11.06 ± 0.63	11.39 ± 0.71

Table 1: Quantitative reproducibility assessment in two brain regions using 1 and 2 averages (7 measurements in 6 rats, per average) at AD=1.3 ms. No significant differences between 1 and 2 averages were found.

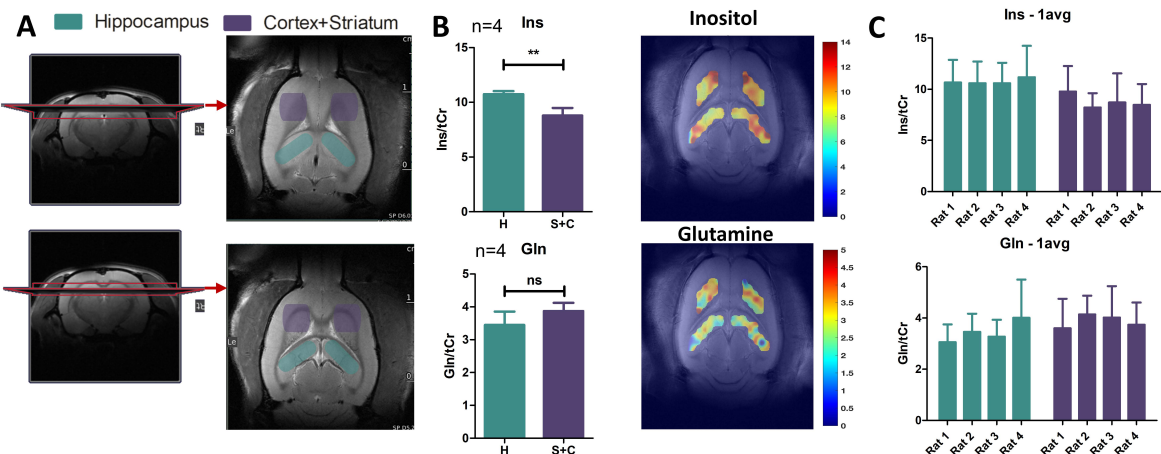


Figure 4: A) Position of the MRSI slice in both axial and coronal views with manually marked brain regions within the slice for illustration purposes only. B) Brain regional differences in resulting concentrations of Ins and Gln (n=4 rats using the quantifications of the MRSI data acquired with 2 averages, on the left) derived from the metabolic maps highlighting the automatic segmentation of the two brain regions (in-vivo example, on the right). Of note, the semi-automatic quality control was not applied to highlight the segmentation outcome. C) Reproducibility of metabolite quantifications (Ins and Gln) between the 4 different animals in the MRSI acquisitions with 1 average. The semi-automatic quality control was applied. A bicubic interpolation was used on the metabolic maps.

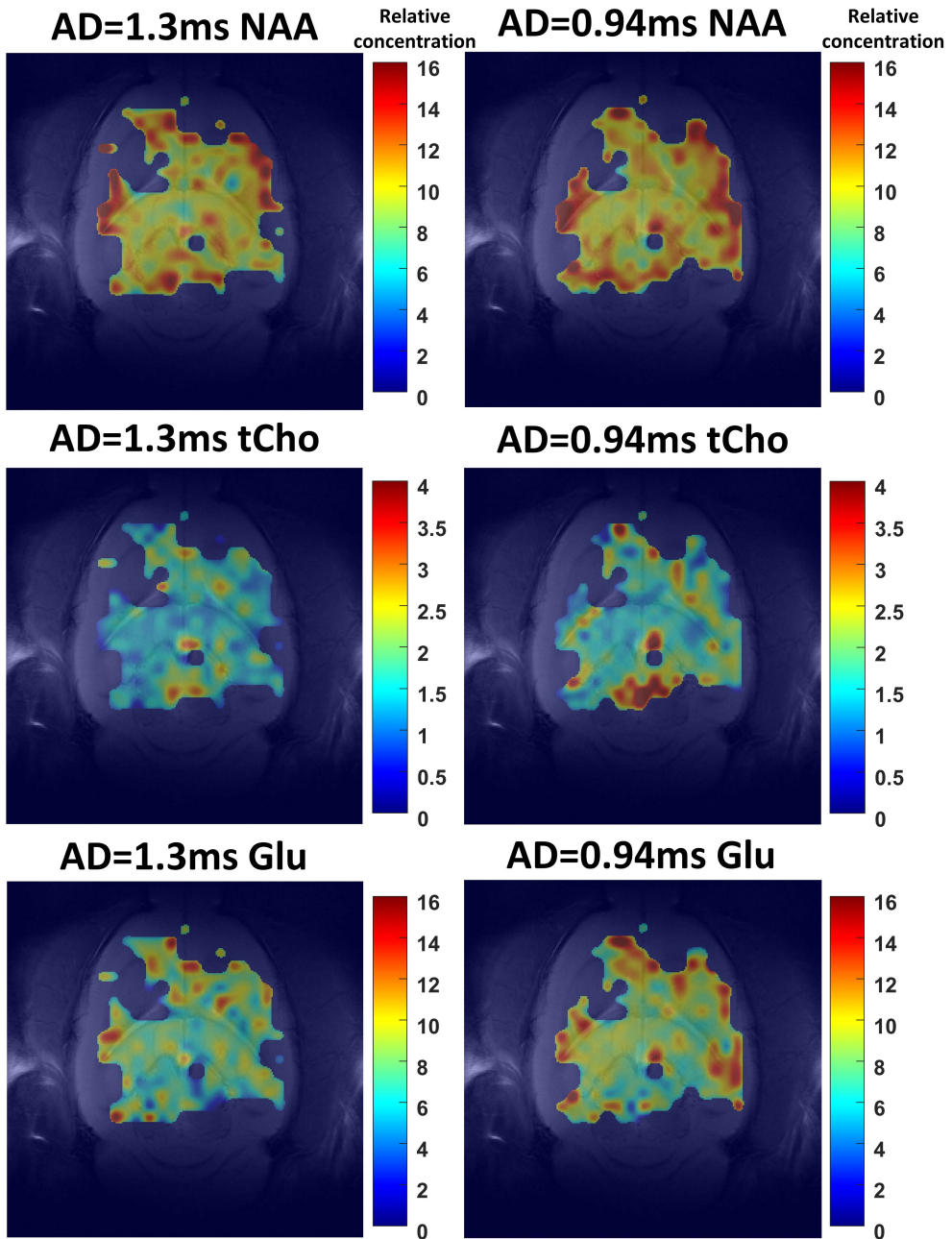


Figure 5: Representative metabolic maps obtained from the LCModel quantification results of the data acquired in one rat with $AD=1.3$ ms (on the left) and $AD=0.94$ ms (on the right), 1 average. The scales correspond to LCModel outputs when referenced to tCr by setting its concentration to $8 \text{ mmol/kg}_{\text{ww}}$. A bicubic convolution interpolation was used on the metabolic maps. The metabolic maps were superimposed to the corresponding anatomical image using the MRS4Brain toolbox.

AD=1.3ms			AD=0.94ms		
*/tCr [mmol/kg _{ww}]	Hippocampus	Striatum + Cortex	*/tCr [mmol/kg _{ww}]	Hippocampus	Striatum + Cortex
NAA	9.84 ± 0.80	9.66 ± 1.14	NAA	8.76 ± 0.78	8.72 ± 0.73
Gln	3.17 ± 0.57	3.85 ± 0.72	Gln	3.32 ± 0.60	3.81 ± 0.57
Glu	7.47 ± 0.87	7.75 ± 1.21	Glu	8.05 ± 0.88	8.62 ± 0.84
Ins	10.94 ± 1.14	8.85 ± 1.08	Ins	9.60 ± 0.77	7.99 ± 0.86
Tau	8.43 ± 0.69	9.60 ± 1.05	Tau	7.72 ± 0.64	8.71 ± 0.92
GPC+PCho	2.02 ± 0.22	2.23 ± 0.30	GPC+PCho	1.68 ± 0.26	1.83 ± 0.32
NAA+NAAG	10.11 ± 0.93	9.84 ± 1.19	NAA+NAAG	8.81 ± 0.79	8.80 ± 0.75

Table 2: Quantitative reproducibility assessment in two brain regions using AD = 1.3 ms and 0.94 ms (4 rats, per AD) with 1 average. No significant differences between ADs were found.

3.3 In-vivo reproducibility

High reproducibility was obtained for the measurement of brain metabolites using ¹H-FID-MRSI, as proposed in our study. The good quality shimming was also kept during the reproducibility studies, with water linewidth ranging between 24-26 Hz over the entire duration of the scans (total of 4 hours, Figure 6), while for the rat scanned at 2 weeks interval the water linewidth ranged between 25-28 Hz for both measurements. Figure 6 illustrates qualitatively the high reproducibility of metabolic mapping in three repeated measurements with 1 average for NAA, tCho and Glu over 4 hours.

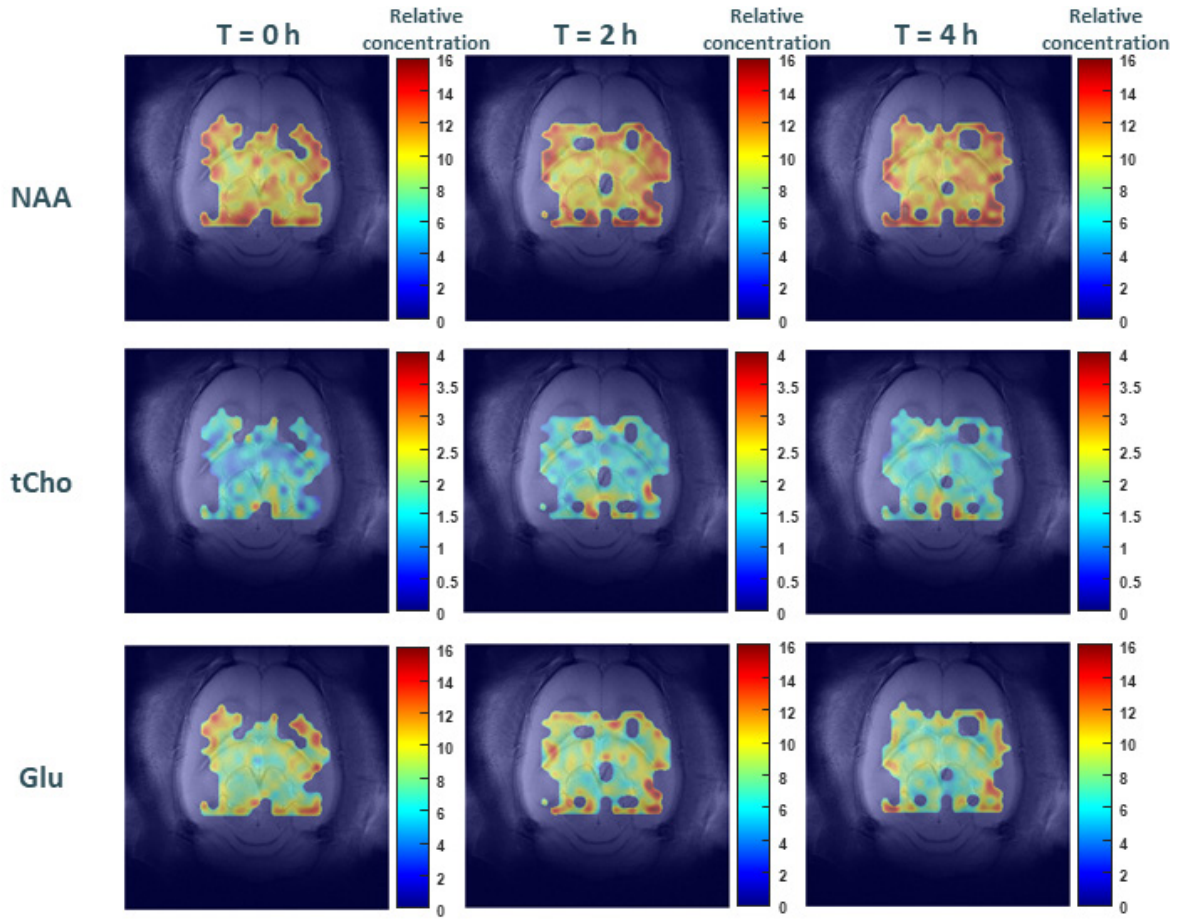


Figure 6: Qualitative reproducibility of metabolic maps illustrated for one experiment where three ^1H -FID-MRSI measurements were performed with 1 average at $\text{AD}=1.3$ ms in the rat brain during 4 hours of acquisition. As can be seen the obtained metabolic maps are reproducible over the 4 hours of acquisition. The scales correspond to LCModel outputs when referenced to tCr by setting its concentration to 8 mmol/kg_{ww}. A bicubic interpolation was used on the metabolic maps. The metabolic maps were superimposed to the corresponding anatomical image using the MRS4Brain toolbox.

4. Discussion

We presented the first implementation and validation of fast ^1H -FID-MRSI in the rat brain at 14.1T with an increased brain coverage, accurate quantification results and robust metabolic maps which enabled us to highlight the well known brain regional distribution of some metabolites in 13 minutes. We showed that our results are reproducible, providing a sound basis for a wider application of ^1H -FID-MRSI in preclinical setting. This was made possible by the use of several technical improvements: implementation of the sequence with a total acquisition time of 13 minutes (i.e. short TR and AD), high quality shimming, water and lipids suppression combined with an in-house developed MRSI processing pipeline specifically designed for such studies. MRS4Brain toolbox is a new MRSI processing pipeline developed for Bruker MRSI data containing several processing steps combined with automatic quality control steps and segmentation tools. Our pipeline eliminated the need to manually classify the data by expert users, to manually overlay the metabolic

maps on the anatomical image and to manually perform brain segmentation concomitantly on anatomical MR images and metabolic maps, which is time-consuming (a minimum of 961/1024 spectra needs to be assessed for each scan), and subjective potentially lowering reproducibility

Ultra-short AD values are particularly useful for the quantification of J-coupled metabolites. In our study using an AD=1.3 ms no J modulation was observed, which simplified spectral quantification substantially, and increased the SNR of J-coupled metabolites⁴. Another advantage of FID-MRSI sequences is the decreased chemical shift displacement artifact, which is increasing proportionally to B_0 , being particularly large for narrow-band, slice-selective RF pulses. As no refocusing pulses are required for FID-MRSI sequences, there is no in-plane chemical shift displacement artifact. At 7T in the human brain, it has been shown that the use of a short, slice-selective excitation RF pulse with high bandwidth and reduced flip-angle reduced the chemical shift displacement artifact to only ~5% per part per million⁴.

MAPSHIM combined with our shimming protocol proved to be efficient leading to an increased brain coverage (not limited to a standard rectangular volume). This resulted in good quality and reliable metabolic maps for a number of metabolites (NAA, tNAA, Glu, tCho, Ins, Gln, Tau etc.). However, as expected a better quality of the acquired MRSI datasets was observed in the center of the MRSI slice, as the usage of surface coils leads to a quality reduction at the edges of the MRSI slice due to the coil sensitivity profile. Furthermore, it is worth pointing towards the necessity of having such automatic quality control steps implemented in a processing pipeline for MRSI datasets, first for a fast and automatic elimination of low quality spectra (i.e. spectra located outside the brain) and also for an overall quality control of the acquired data, as “bad” quality data can be excluded directly without spending time in further processing them (Supplementary Figure 1).

We have furthermore decreased the AD to 0.94 ms, showing the feasibility of acquiring and fitting these datasets with similar concentration estimates and brain coverage between the two ADs. This reduction in AD is potentially beneficial for low concentration and J-coupled metabolites as the 1st order phase evolution will be smaller and less T₂* evolution will occur. The quantification of low-concentration metabolites (i.e. GABA, Asp, PE, Asc, GSH) was not shown due to the smaller number of voxels reliably quantified and thus needing further improvements, either by reducing the AD or by improving the measurement of MM using ¹H-FID-MRSI acquisition protocols combined with a double inversion module and increased number of averages. Indeed, we observed that single inversion recovery leads to important residual metabolites in ¹H-FID-MRSI datasets which were difficult to identify mainly due to the low SNR of MM spectra, water residuals and a complicated spectral pattern imposed by the 1st order phase evolution during the AD. Therefore, for the MRSI data acquired with AD=1.3 ms, we used an MM spectrum acquired with an ultra-short TE STEAM sequence where residual metabolites

were reliably identified and with longer TR than for the ^1H -FID-MRSI acquisitions, leading to the possibility to neglect relaxation effects. On the other hand, for AD=0.94 ms the double inversion recovery module combined with the higher spatial resolution led to a better suppression of metabolite and water residuals, respectively. Both single and double inversion recovery modules are recommended for the measurement of MM spectra in-vivo, while the double inversion recovery modules seem to be more widely used for ^1H -FID-MRSI^{4,25,26}. The current study supports this trend by showing that the double inversion recovery modules seem to be better suited for MRSI acquisitions.

Ala and Lac were not reported due to possible lipid contamination/lipid removal even though overall good lipid suppression was obtained for the ^1H -FID-MRSI datasets. In human studies at 7T, different groups have addressed this issue for ^1H -MRSI, using OVS, inversion recovery, frequency-selective suppression or suppression based on B_1 shimming approaches or by improving the point-spread function by increasing the matrix size and applying spatial Hamming filtering^{4,5,27-30}. In our study, the lipid suppression was enhanced by the usage of the SVD-based lipid suppression¹⁶. As saturation slabs were also used during the acquisition of the MRSI datasets, the α parameter in the SVD-based lipid suppression was set manually to 0.5.

The short TR used in our study led to short acquisition times (i.e. 13 minutes for a 31×31 MRSI matrix) but also to stronger T_1 weighting. Adjusting the Ernst excitation flip angle led to a reduction in the T_1 weighting as previously shown at 7T in the human brain⁴. Furthermore, we used tCr as internal reference during the quantification step as metabolite ratios are less sensitive to flip angle errors and T_1 weighting. Of note, when correcting for T_1 relaxation times differences in metabolite T_1 relaxation times and the different T_1 values of resonances originating from the same molecule (i.e. NAA and CH_2 groups³¹) should be taken into account.

Limitations & Future steps

The quantifications were limited by the brain coverage of the 2-loop surface RF coil used with potential B_1 inhomogeneities towards the edges of the metabolic maps, and by variable B_0 homogeneity in some brain regions leading to metabolic maps which do not fully cover the brain as in human studies. As such, future studies will focus on improving both the RF excitation homogeneity and RF reception coverage, potentially by using surface transceiver phased arrays, or by combining surface-receive with volume-transmit RF coils, whose compatibility regarding the power deposition in ^1H -FID-MRSI at high duty cycle needs to be evaluated. The increased SNR and brain coverage would be potentially beneficial also for static field shimming. In parallel, further reducing the TR and consequently adapting the water and lipid suppression efficiency for shorter TRs together with the implementation of a concentric rings encoding^{1,32} would allow faster acquisitions and potentially enable 3D encoding³³.

Future studies will also investigate the efficiency of lipid suppression using metabolite-lipid orthogonality and the best compromise between the amount of lipid contamination (depending on the RF coils used and presence or not of saturation bands in the sequence) and the rank of the basis for the approximated lipid subspace. In the present study, tCr was used as an internal reference. In the next step we will focus on correcting for T₁ relaxation times using previously published values³¹. Furthermore, improvements in the fitting process will be performed (i.e. new MM acquisitions using double inversion recovery and higher spatial resolution) to improve the quantification of low-concentration metabolites, and also investigate the fluctuations in metabolite concentrations in some metabolic maps. Some metabolites showed higher concentration towards the edges of the maps, which could be due to some technical issues (surface coils induced B₁ inhomogeneities, interpolation of the maps, fitting issues, etc.) or to “real” variations/changes in some fine brain regions, something needing further investigations (Supplementary Figures 5 and 6). Of note, these spectra passed the quality criteria and they are displayed in Supplementary Figure 5. By further reducing the AD to ~0.7 ms we would also be able to predict the missing FID points due to the acquisition delay as done previously^{6,16} and thus eliminate the 1st order phase distortions.

5. Conclusion

In this study, we demonstrated that the increased SNR and spectral resolution at 14.1T can be translated into high spatial resolution in ¹H-FID-MRSI of the rat brain in 13 minutes, using the sequence and processing pipeline described herein. High reproducibility was achieved in several brain regions together with the detection of brain regional differences, as illustrated by the in-vivo measurements. As such, high-resolution ¹H-FID-MRSI at 14.1T provided robust, reproducible and high-quality metabolic mapping of brain metabolites with significantly reduced technical limitations using AD of 1.3 and 0.94 ms. The short duration of the metabolite acquisition (i.e. 13 minutes) can be easily translated into biomedical applications in different animal models where brain regional evolution of metabolites is questioned during disease evolution and thus provide insights into the pathogenesis of major neurological diseases and improve the understanding of the basic neurochemical mechanisms involved in brain metabolism.

Data availability:

The *MRS4Brain toolbox* version v.0.1 is currently finalized and will be made available on the following repository: <https://github.com/AlvBrayan/MRS4Brain-toolbox> during the revision process. Experimental data used in the present manuscript will also be made available on the same repository during the revision process. Finally, a live demo on how to acquire in-vivo ¹H-FID-MRSI datasets will be posted on the webpage: Standardized Preclinical MRS: A Multi-Center Study – MRS4BRAIN - EPFL

Acknowledgments:

This work was supported by the Swiss National Science Foundation award n° 201218 and 207935 and by the Center for Biomedical Imaging of the UNIL, UNIGE, HUG, CHUV, EPFL, the Leenaards and Jeantet Foundations. The authors thank Dr. Katarzyna Pierzchala for building the phantom and the veterinary staff at CIBM MRI EPFL AIT for support during experiments.

References:

1. Bogner W, Otazo R, Henning A. Accelerated MR spectroscopic imaging—a review of current and emerging techniques. *NMR Biomed.* 2021;34(5):e4314. doi:10.1002/nbm.4314
2. De Graaf RA. *In Vivo NMR Spectroscopy : Principles and Techniques*. 2nd ed. Chichester, West Sussex, England ; Hoboken, NJ : John Wiley & Sons; 2007.
3. Maudsley AA, Andronesi OC, Barker PB, et al. Advanced magnetic resonance spectroscopic neuroimaging: Experts' consensus recommendations. *NMR Biomed.* 2021;34(5):e4309. doi:10.1002/nbm.4309
4. Bogner W, Gruber S, Trattnig S, Chmelik M. High-resolution mapping of human brain metabolites by free induction decay ¹H MRSI at 7 T. *NMR Biomed.* 2012;25(6):873-882. doi:10.1002/nbm.1805
5. Henning A, Fuchs A, Murdoch JB, Boesiger P. Slice-selective FID acquisition, localized by outer volume suppression (FIDLOVS) for 1H-MRSI of the human brain at 7 T with minimal signal loss. *NMR Biomed.* 2009;22(7):683-696. doi:10.1002/nbm.1366
6. Nassirpour S, Chang P, Henning A. High and ultra-high resolution metabolite mapping of the human brain using ¹ H FID MRSI at 9.4T. *NeuroImage*. 2018;168:211-221. doi:10.1016/j.neuroimage.2016.12.065
7. Lanz B, Abaei A, Braissant O, et al. Magnetic resonance spectroscopy in the rodent brain: Experts' consensus recommendations. *NMR Biomed.* 2021;34(5):e4325. doi:10.1002/nbm.4325
8. Mlynárik V, Kohler I, Gambarota G, Vaslin A, Clarke PGH, Gruetter R. Quantitative proton spectroscopic imaging of the neurochemical profile in rat brain with microliter resolution at ultra-short echo times. *Magn Reson Med.* 2008;59(1):52-58. doi:10.1002/mrm.21447

9. Hangel G, Strasser B, Považan M, et al. Ultra-high resolution brain metabolite mapping at 7 T by short-TR Hadamard-encoded FID-MRSI. *NeuroImage*. 2018;168:199-210. doi:10.1016/j.neuroimage.2016.10.043
10. Delgado-Goñi T, Ortega-Martorell S, Ciezka M, et al. MRSI-based molecular imaging of therapy response to temozolomide in preclinical glioblastoma using source analysis. *NMR Biomed*. 2016;29(6):732-743. doi:10.1002/nbm.3521
11. Cudalbu C. In vivo studies of brain metabolism in animal models of Hepatic Encephalopathy using ¹H Magnetic Resonance Spectroscopy. *Metab Brain Dis*. 2013;28(2):167-174. doi:10.1007/s11011-012-9368-9
12. Geppert C, Dreher W, Leibfritz D. PRESS-based proton single-voxel spectroscopy and spectroscopic imaging with very short echo times using asymmetric RF pulses. *Magn Reson Mater Phys Biol Med*. 2003;16(3):144-148. doi:10.1007/s10334-003-0016-6
13. Juchem C, Logothetis NK, Pfeuffer J. High-resolution ¹H chemical shift imaging in the monkey visual cortex. *Magn Reson Med*. 2005;54(6):1541-1546. doi:10.1002/mrm.20687
14. Topping GJ, Hundshammer C, Nagel L, et al. Acquisition strategies for spatially resolved magnetic resonance detection of hyperpolarized nuclei. *Magn Reson Mater Phys Biol Med*. 2020;33(2):221-256. doi:10.1007/s10334-019-00807-6
15. Tkáč I, Starčuk Z, Choi IY, Gruetter R. In vivo ¹H NMR spectroscopy of rat brain at 1 ms echo time. *Magn Reson Med*. 1999;41(4):649-656. doi:10.1002/(SICI)1522-2594(199904)41:4<649::AID-MRM2>3.0.CO;2-G
16. Klauser A, Courvoisier S, Kasten J, et al. Fast high-resolution brain metabolite mapping on a clinical 3T MRI by accelerated H-FID-MRSI and low-rank constrained reconstruction. *Magn Reson Med*. 2019;81(5):2841-2857. doi:10.1002/mrm.27623
17. Barkhuijsen H, De Beer R, Van Ormondt D. Improved algorithm for noniterative time-domain model fitting to exponentially damped magnetic resonance signals. *J Magn Reson* 1969. 1987;73(3):553-557. doi:10.1016/0022-2364(87)90023-0
18. Mosso J, Simicic D, Şimşek K, Kreis R, Cudalbu C, Jelescu IO. MP-PCA denoising for diffusion MRS data: promises and pitfalls. *NeuroImage*. 2022;263:119634. doi:10.1016/j.neuroimage.2022.119634
19. Barrière DA, Magalhães R, Novais A, et al. The SIGMA rat brain templates and atlases for multimodal MRI data analysis and visualization. *Nat Commun*. 2019;10(1):5699. doi:10.1038/s41467-019-13575-7
20. Starčuk Z, Starčuková J. Quantum-mechanical simulations for in vivo MR spectroscopy: Principles and possibilities demonstrated with the program NMRScopeB. *Anal Biochem*. 2017;529:79-97. doi:10.1016/j.ab.2016.10.007
21. Govindaraju V, Young K, Maudsley AA. Proton NMR chemical shifts and coupling constants for brain metabolites. *NMR Biomed*. 2000;13(3):129-153. doi:10.1002/1099-1492(200005)13:3<129::AID-NBM619>3.0.CO;2-V
22. Govind V, Young K, Maudsley AA. Corrigendum: Proton NMR chemical shifts and coupling constants for brain metabolites. Govindaraju V, Young K, Maudsley AA, NMR Biomed. 2000; 13: 129–153. *NMR Biomed*. 2015;28(7):923-924. doi:10.1002/nbm.3336

23. Simicic D, Rackayova V, Xin L, et al. In vivo macromolecule signals in rat brain 1H-MR spectra at 9.4T: Parametrization, spline baseline estimation, and T2 relaxation times. *Magn Reson Med.* 2021;86(5):2384-2401. doi:10.1002/mrm.28910
24. Tkáč I, Rao R, Georgieff MK, Gruetter R. Developmental and regional changes in the neurochemical profile of the rat brain determined by in vivo 1H NMR spectroscopy. *Magn Reson Med.* 2003;50(1):24-32. doi:10.1002/mrm.10497
25. Považan M, Hangel G, Strasser B, et al. Mapping of brain macromolecules and their use for spectral processing of 1 H-MRSI data with an ultra-short acquisition delay at 7 T. *NeuroImage.* 2015;121:126-135. doi:10.1016/j.neuroimage.2015.07.042
26. Považan M, Strasser B, Hangel G, et al. Simultaneous mapping of metabolites and individual macromolecular components via ultra-short acquisition delay 1H MRSI in the brain at 7T. *Magn Reson Med.* 2018;79(3):1231-1240. doi:10.1002/mrm.26778
27. Hetherington HP, Avdievich NI, Kuznetsov AM, Pan JW. RF shimming for spectroscopic localization in the human brain at 7 T. *Magn Reson Med.* 2010;63(1):9-19. doi:10.1002/mrm.22182
28. Balchandani P, Spielman D. Fat suppression for 1H MRSI at 7T using spectrally selective adiabatic inversion recovery. *Magn Reson Med.* 2008;59(5):980-988. doi:10.1002/mrm.21537
29. Boer VO, Siero JCW, Hoogduin H, van Gorp JS, Luijten PR, Klomp DWJ. High-field MRS of the human brain at short TE and TR. *NMR Biomed.* 2011;24(9):1081-1088. doi:10.1002/nbm.1660
30. Tkáč I, Deelchand D, Dreher W, et al. Water and lipid suppression techniques for advanced 1H MRS and MRSI of the human brain: Experts' consensus recommendations. *NMR Biomed.* 2021;34(5):e4459. doi:10.1002/nbm.4459
31. Cudalbu C, Mlynárik V, Xin L, Gruetter R. Comparison of T1 relaxation times of the neurochemical profile in rat brain at 9.4 tesla and 14.1 tesla. *Magn Reson Med.* 2009;62(4):862-867. doi:10.1002/mrm.22022
32. Hingerl L, Bogner W, Moser P, et al. Density-weighted concentric circle trajectories for high resolution brain magnetic resonance spectroscopic imaging at 7T. *Magn Reson Med.* 2018;79(6):2874-2885. doi:10.1002/mrm.26987
33. Hingerl L, Strasser B, Moser P, et al. Clinical High-Resolution 3D-MR Spectroscopic Imaging of the Human Brain at 7 T. *Invest Radiol.* 2020;55(4):239. doi:10.1097/RLI.0000000000000626

Supplementary File

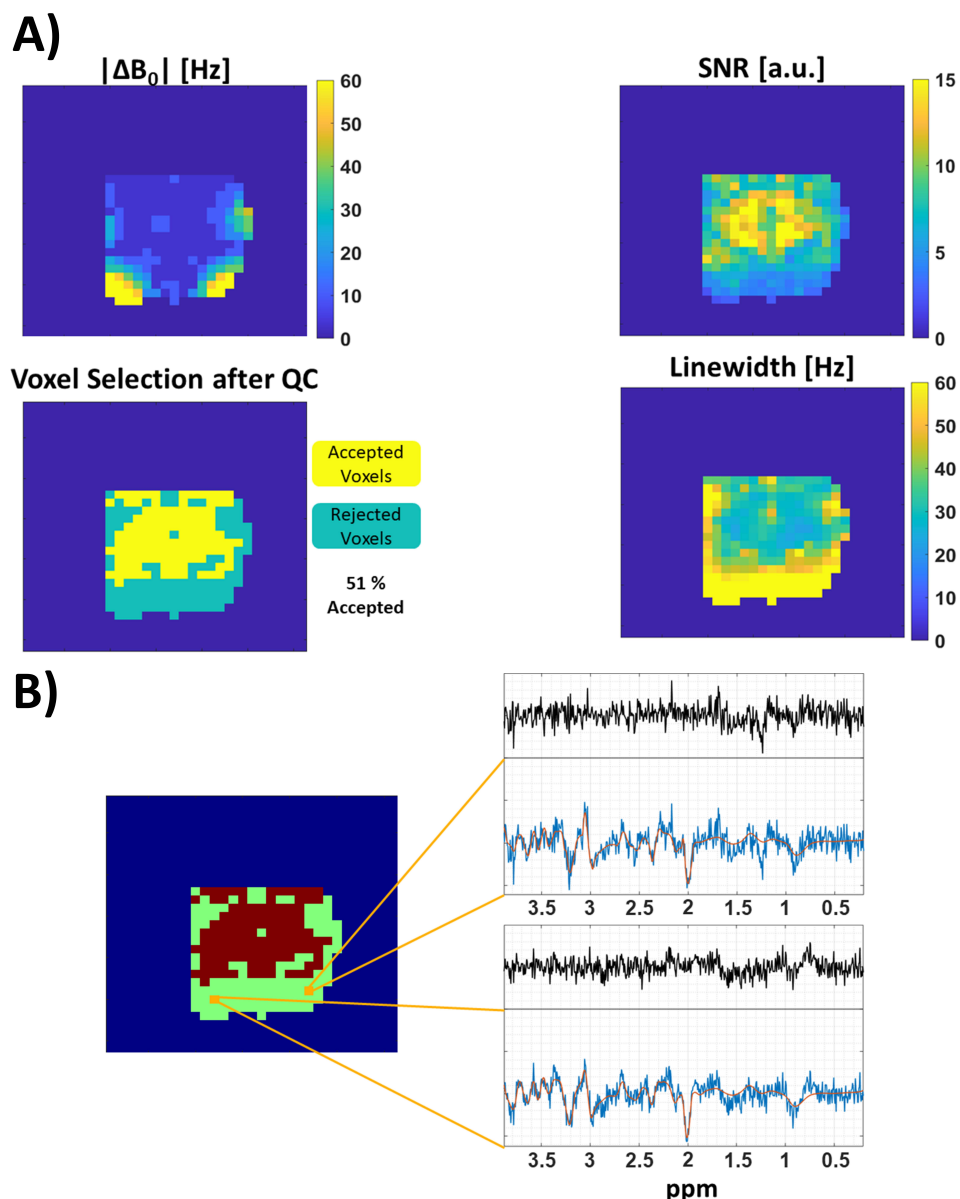
Methods: two-compartment phantom

To test the precision of the ^1H -FID-MRSI sequence and its ability to separate metabolic profiles from different brain regions we built a two-compartment phantom. The phantom consisted of two syringes; a small syringe (5 ml) positioned inside a big syringe (50 ml). The small syringe was filled with a high concentration (~50 mM) of Cr with 1 $\mu\text{mol}/\text{ml}$ gadolinium (Gd, Diethylenetriaminepentaacetic acid gadolinium(III) dihydrogen salt hydrate, Sigma-Aldrich, 381667) dissolved in phosphate buffer saline (PBS) and the big syringe was filled with a high concentration (~40 mM) of Glu with 1 $\mu\text{mol}/\text{ml}$ Gd dissolved in PBS. Both ^1H -FID and PRESS-MRSI acquisitions were performed with the following parameters:

- PRESS-MRSI: TE = 12.7 ms, TR = 2000 ms, one average, 31×31 matrix in a FOV = $24 \times 24 \text{ mm}^2$ leading to a total scan time of 32 minutes. The VOI of $10 \times 10 \times 2 \text{ mm}^3$ was centered in the phantom (positioned in the same slice used for ^1H -FID-MRSI).
- ^1H -FID-MRSI: acquisition delay AD = 1.3 ms, TR = 812 ms, one average, matrix size 31×31 in a FOV = $24 \times 24 \text{ mm}^2$ (slice positioned to contain the PRESS VOI) leading to a total acquisition time of 13 minutes.

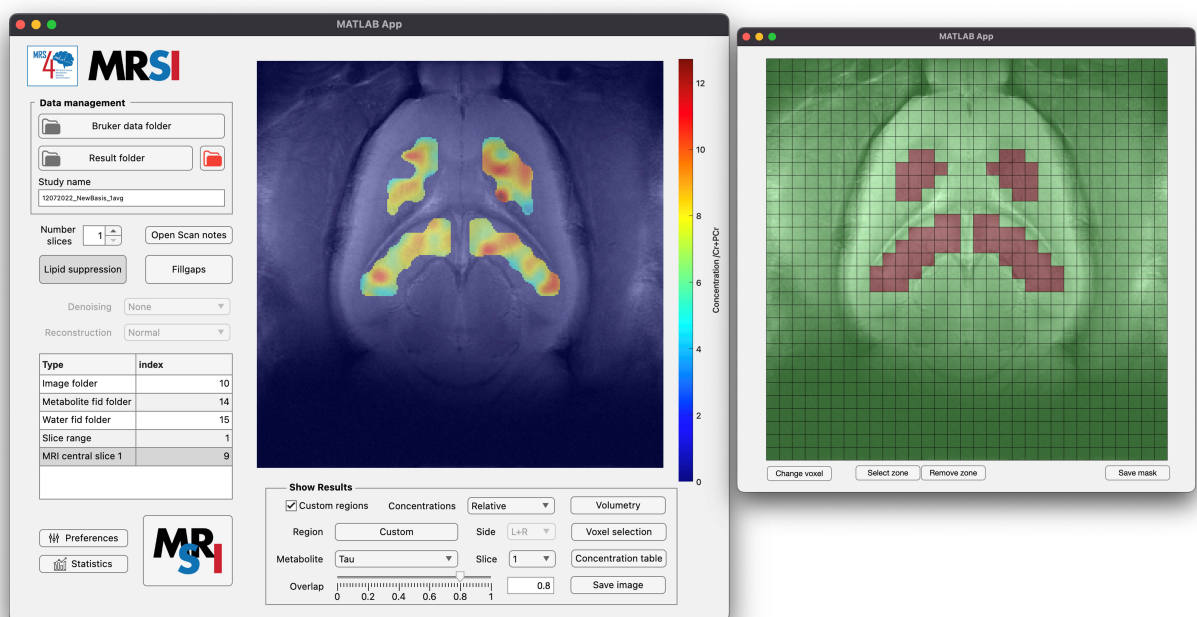
Supplementary Figure 1: A) Representative water ΔB_0 , NAA SNR, water linewidth and voxel selection after QC maps obtained after the application of the water power map on the full ^1H -FID-MRSI matrix (QC - semi-automatic quality control applied in step 7 of the MRSI processing pipeline). Only voxels located within the brain, as determined from the water power mask, are kept, while in the QC map the remaining “bad” quality voxels are further removed during the QC steps, see part B).

B) Example of “bad” quality voxels removed by the semi-automatic quality control presented in step 7 of the MRSI processing pipeline. As can be seen these voxels show the presence of brain metabolites and not only noise, no lipid contamination is observed, however broad linewidths are visible.



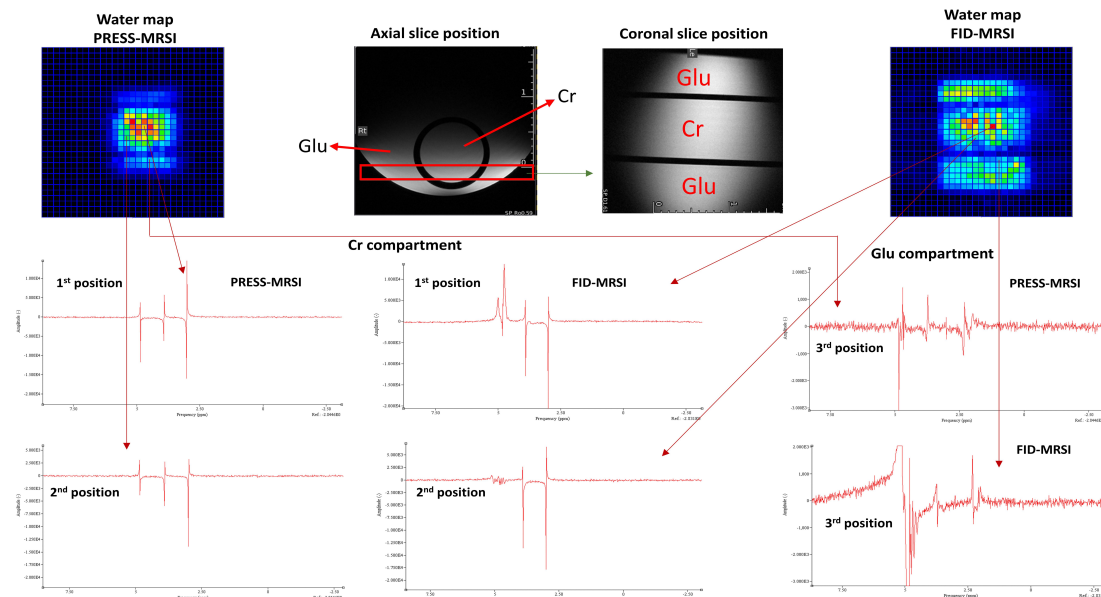
Supplementary Figure 2: Representative screenshot of the *MRS4Brain toolbox* incorporating the pipeline to process, quantify, display and evaluate MRSI data from a Bruker MR scanner. Version v.0.1 of the software runs in MATLAB and is available here: <https://github.com/AlvBrayan/MRS4Brain-toolbox>.

Additional features not highlighted in the manuscript are available in the MRSI processing pipeline: possibility to process X-nuclei MRSI data sets, change or create new Control files for LCModel fitting based on the parameters used herein for quantification (Preferences tab), open PDF files available in the acquisition folder, process multi-slice MRSI data sets, customize the specific processing techniques to be employed in the pipeline (Lipid suppression, Fillgaps, non cartesian Reconstruction), merge brain regions based on the automatic segmentation, calculate the brain volumetry, display concentration maps and information (mean and standard deviation). At the current moment, features with regards to reconstruction are still in the process of being added to the GUI and will be made available later on GitHub.

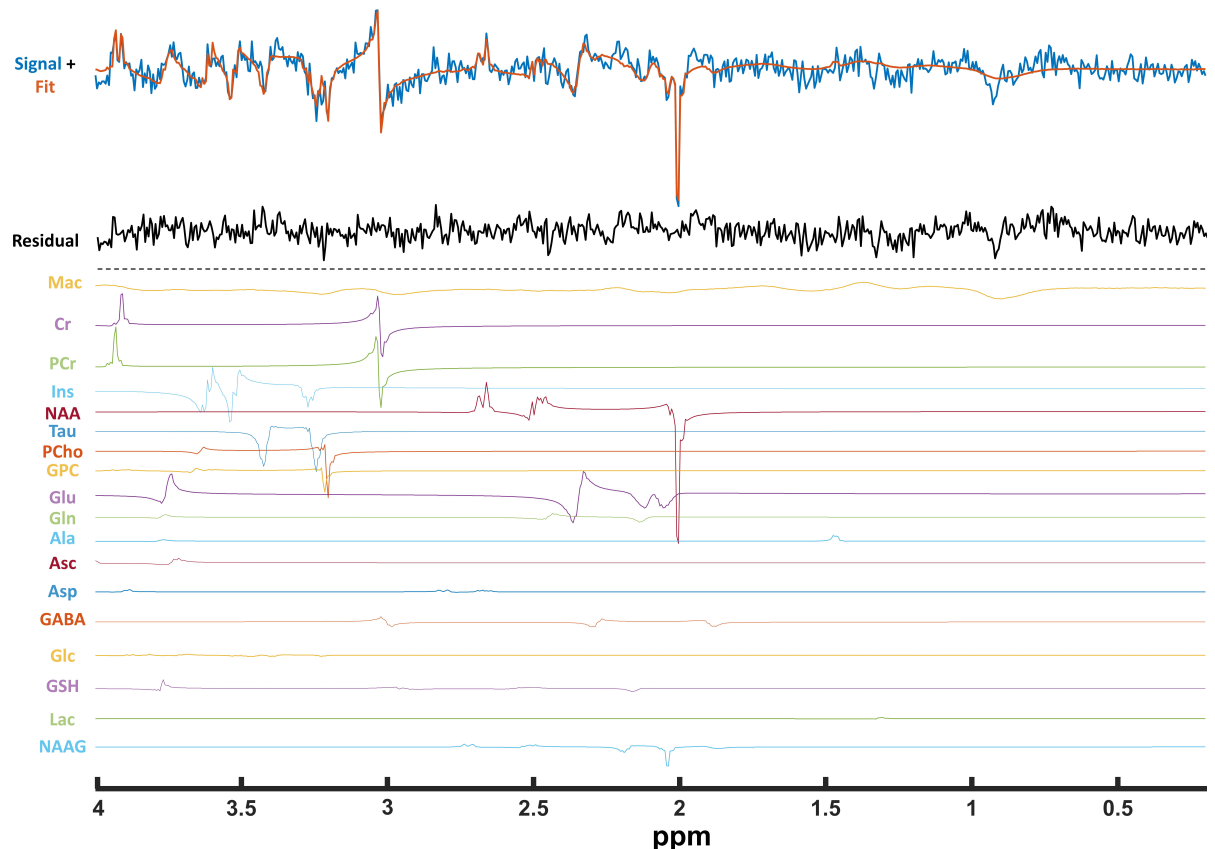


Supplementary Figure 3: Two compartment phantom ^1H -FID-MRSI vs. PRESS- ^1H -MRSI. **(up)** The water map provided by the jMRUI MRSI tool resulting from the PRESS-MRSI acquisition is shown on the left while the water map resulting from the ^1H -FID-MRSI acquisition is shown on the right. The T_2 -weighted Turbo-RARE images of the phantom in the coronal (centered on the MRSI slice) and axial positions are shown in the middle. **(down)** Spectra from three different positions (locations) in the matrix acquired with the two methods (PRESS and FID) are displayed for comparison (always the identical position for both sequences).

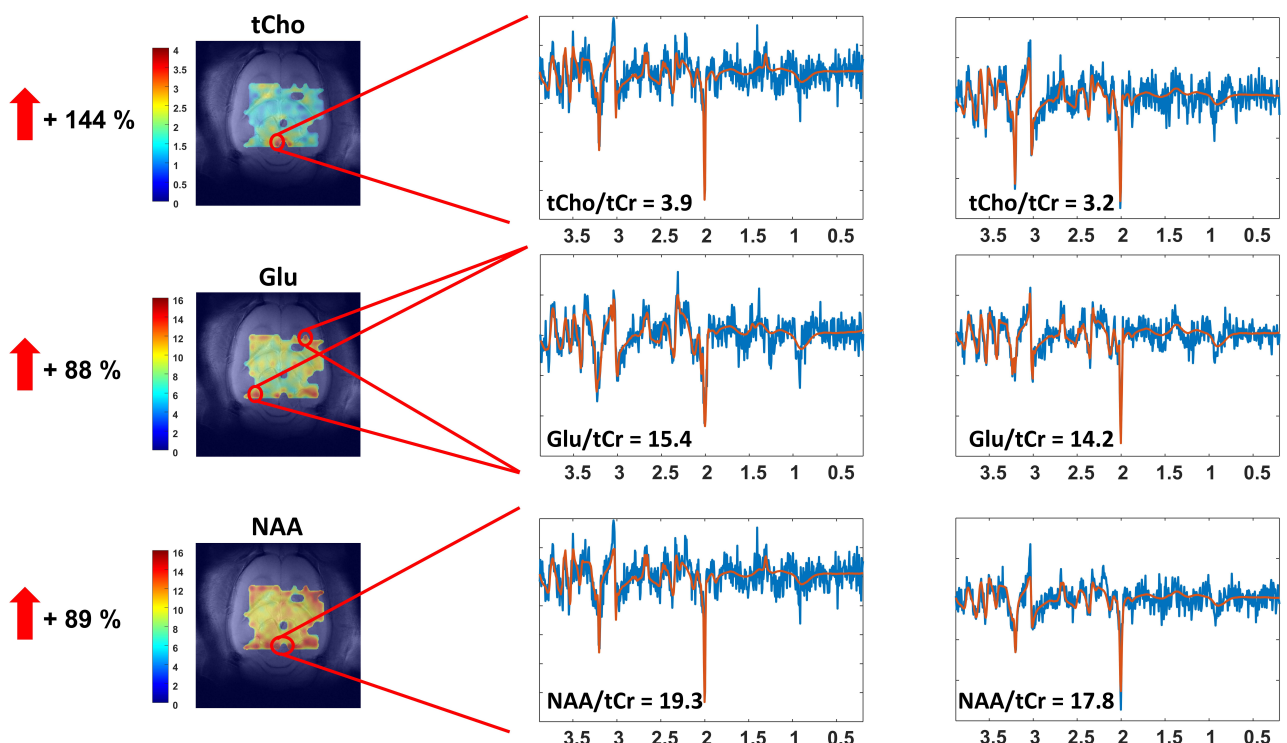
The “pure” Cr spectra were measured from the nominal voxels located in the Cr compartment, while the spectra from the Glu compartment (on the border with Cr compartment) contained a very minimal Cr contamination. This small Cr signal most probably comes from contamination of the Glu compartment during phantom preparation, rather than from the imperfect localization, supported also by the water maps. Of note, the Glu compartment showed a higher water residual which can further be removed in the processing step using HSVD.



Supplementary Figure 4: Example of LCModel fit, using the simulated metabolite basis-set and in-vivo measured MM (Mac), showing an in-vivo spectrum at AD = 1.3 ms (blue), the LCModel fit (red), fit residual, the estimated spectra of individual metabolites and MM included in the basis-set.



Supplementary Figure 5: Example of spectra in some metabolic maps showing high concentrated metabolites towards the edges of the maps as shown by the red arrows on the left part of the image. As can be seen these spectra passed the quality criteria.



Supplementary Figure 6: Representative metabolic maps with and without interpolation obtained from the LCModel fitting results of the data acquired in one rat. As can be seen the interpolation might have accentuated the metabolite fluctuations in the edges of the metabolic maps. The scales correspond to LCModel outputs when referenced to tCr by setting its concentration to 8 mmol/kg_{ww}. A bicubic convolution interpolation was used on the metabolic maps. The metabolic maps were superimposed to the corresponding anatomical image using the *MRS4Brain toolbox*.

